Applied Catalysis A, General xxx (xxxx) 119292

Contents lists available at ScienceDirect

Applied Catalysis A, General

journal homepage: www.elsevier.com/locate/apcata

Influence of residual chlorine on Ru/TiO_2 active sites during CO_2 methanation

James M. Crawford [a,*], Brittney E. Petel [a], Mathew J. Rasmussen [a], Thomas Ludwig [c], Elisa M. Miller [b], Sawyer Halingstad [a], Sneha A. Akhade [c], Simon H. Pang [c], Matthew M. Yung [a]

[a] Catalytic Carbon Transformation and Scale-up Center, National Renewable Energy Laboratory, Golden, CO 80401, USA
[b] Materials, Chemical, and Computational Science Directorate, National Renewable Energy Laboratory, Golden, CO 80401, USA
[c] Materials Science Division, Lawrence Livermore National Laboratory, Livermore, CA 94550, USA

ARTICLE INFO

Keywords:
Methanation
Sabatier reaction
CO_2 Utilization
Ruthenium
Titania
Heterogeneous catalysis

ABSTRACT

Titania-supported ruthenium (Ru/TiO_2) is an established catalyst for the hydrogenation of carbon dioxide to methane (Sabatier reaction). Chlorine contamination, owed to the $RuCl_3$ precursor, is demonstrated to have a detrimental impact on methanation activity. After calcination and reduction the catalyst contains residual chlorine, shown by XPS. An aqueous ammonia wash removes Cl without leaching Ru. The washed catalysts exhibit improvements in CH_4 site-time yields. Low Ru loading catalysts encounter the greatest activity enhancements after washing (~4.5–fold). DFT calculations indicate that chlorine and CO_2 directly compete for adsorption on Ru step sites, with Cl impeding the adsorption of CO_2 at under-coordinated sites and at higher Cl coverages. H_2-chemisorption/TPR show that Cl removal lowers the onset of low temperature H_2 dissociation on Ru. DRIFTS provide evidence that the removal of Cl facilitates low temperature dissociative binding of CO_2, indicated by the formation of surface bound linear CO species.

1. Introduction

Methanation, also known as the Sabatier reaction, has been the focus of intense study for integration with renewable hydrogen and energy (wind/solar) as a product for scavenged atmospheric carbon dioxide [1]. Methane is a favorable equilibrium product below 300 °C when carbon dioxide is combined with hydrogen: $CO_2 + 4H_2 \rightarrow CH_4 + 2H_2O$. Finding high activity catalysts that preform methanation at low temperatures is important to reduce the energy consumption of the Sabatier process [1]. Catalyst-support combinations have been recently reviewed in detail for the methanation reaction [2]. Ruthenium-supported catalysts consistently show the highest activity at low temperature (~200 °C). Furthermore, Ru/TiO_2 catalysts exhibit lower temperature light-off than Ru supported on other refractory metal oxides (*e.g.*, SiO_2, ZrO_2, and Al_2O_3). In a seminal example, Grätzel and coworkers demonstrated that Ru/TiO_2 catalysts were active for methanation, even at room temperature [3]. More recently, it has been established that the thermal history [4], crystalline phase of the support [5], metal nanoparticle size [6], metal-support interaction [7], exposed crystal facets [8], and the presence of support-grafted ligands [9,10] have significant impacts on the conversion and selectivity during carbon dioxide reduction.

Additionally, the choice of metal precursors can impact the activity of the catalyst. Ruthenium based precursors used to synthesize methanation catalysts often include ruthenium chloride ($RuCl_3$), ruthenium nitrosyl nitrate ($Ru(NO)(NO_3)_3$), and ruthenium acetylacetonate ($Ru(acac)_3$). $RuCl_3$ is the starting point for the majority of Ru chemistries and represents the most industrially prepared Ru complex [11]. $Ru(NO)(NO_3)_3$ and $Ru(acac)_3$ are obtained through excess ligand exchange of $RuCl_3$ in a solution of acid or base [11]. Thus, additional processing steps are required to obtain ruthenium nitrate or acetylacetonate salts. The added synthetic complexity is captured in the cost of the precursors ($RuCl_3$ ~ \$60·g Ru^{-1}, $Ru(NO)(NO_3)_3$ ~ \$170·g Ru^{-1}, $Ru(acac)_3$ ~ \$400·g Ru^{-1}; Data retrieved from Sigma-Aldrich on May 8th, 2023). Therefore, if sufficient activity is attainable from $RuCl_3$ derived catalysts, significant synthetic cost advantages could be realized. Currently, no systematic studies relating ruthenium precursors to methanation activity are available. However, some work has been done comparing ruthenium precursors for ammonia synthesis catalysis. Nanba and coworkers generated Ru/CeO_2 catalysts using nine ruthenium precursors. While no morphological impacts were observed when changing the ruthenium precursor, the catalytic activity trended well with reducibility (probed by temperature programmed reduction). Their study showed that the catalyst derived from $RuCl_3$ had lower per-

* Corresponding author.

https://doi.org/10.1016/j.apcata.2023.119292
Received 28 March 2023; Received in revised form 17 May 2023; Accepted 3 June 2023
0926-860/© 20XX

formance when compared to $Ru(NO)(NO_3)_3$ and $Ru(acac)_3$ [12]. Wei and coworkers found that Ru/Al_2O_3 ammonia synthesis catalysts were negatively impacted by the presence of residual or added chlorine. The lower activity was attributed to site-blocking at hydrogen adsorption sites. It was also noted that Cl did not impact the resultant metal nanoparticle size [13]. The impact of residual chlorine has also been studied in the context of ruthenium catalysts for the hydrogenation of aromatics where residual chlorine had a poisoning impact on the Ru/Al_2O_3 catalyst. The authors showed that removal of Cl through washing recovered the desired hydrogenation activity [14].

While early descriptions of Ru/TiO_2 methanation catalysts alluded to the importance of Cl removal [3,15], no systematic evaluation of residual chlorine has been undertaken in the context of continuous methanation. Among Ru/TiO_2 methanation studies, catalyst preparations can be divided into three main groups: (i) chlorine-containing precursors are used without washing [16–20], (ii) chlorine-containing precursors are used with a subsequent washing step [3,7,15,21,22], or (iii) chlorine-free precursors are used [23,24]. Thus, a systematic evaluation of chlorine contamination on Ru/TiO_2 is needed to clarify activity trends in the existing literature, to confirm the necessity of Cl removal when generating catalyst from metal chlorides, and to reduce the cost of future methanation catalysts.

In this report, Cl removal (*via* washing) is demonstrated to have a positive impact on low temperature methanation over Ru/TiO_2 catalysts. The morphology of the catalyst was unaffected by Cl removal. The methane formation rates increased dramatically for all washed catalysts as compared to unwashed catalysts. *In situ* diffuse reflectance infrared spectroscopy demonstrated that Cl blocks the adsorption and dissociation of CO_2 to CO in H_2 at Ru active sites, which was corroborated by density functional theory calculations and described in this contribution. Additionally, Cl inhibited hydrogen chemisorption and low temperature reduction of the metal sites.

2. Materials and methods

2.1. Chemicals and supplies

Ruthenium chloride ($RuCl_3 \cdot 2.78\ H_2O$, Alfa-Aesar, 99.9 % trace metal basis), hydration determined by thermogravimetric analysis (TGA, Fig. S1) [25], titania (TiO_2, Johnson Matthey, 500 μm spheres) and ultrapure water were used for incipient wetness impregnation (18 MΩ-cm). An aqueous ammonia solution (NH_4OH, Sigma-Aldrich, 28–30 %) was used to wash the catalyst. Silver nitrate ($AgNO_3$, Sigma-Aldrich, > 99.0 %, ACS reagent) was used to evaluate the presence of Cl in the effluent ultrapure water after the wash. Quartz chips (SiO_2, Saint-Gobain, 800–1000 μm) were used to dilute the catalyst in activity tests. Quartz wool (Technical Glass Products, 5–15 μm fibers) was used to support the catalyst during chemisorption studies. All gases were supplied by Matheson as ultra-high purity or certified gas mixtures.

2.2. Catalyst synthesis

Ru/TiO_2 catalysts were formed using incipient wetness impregnation (IWI). The appropriate solution volume (V_{IWI}) was calculated by Eq. 1,

$$V_{IWI} = V_p * m * I \tag{1}$$

where the total pore volume, V_p, was measured by cryogenic nitrogen physisorption (N_2-physisorption), m was the mass of the support, and I was the number of impregnation treatments ($I = 2$ for the double impregnation, employed here). $RuCl_3$ was added to the solution volume of water and stirred until dissolved. Half of the solution was then slowly added onto the dry TiO_2 support under vigorous stirring. The mixture was then dried at 110 °C. Once dry, the same procedure was repeated. After drying, catalysts were calcined at 300 °C (ramp = 10 °C·min^{-1}, hold = 3 h) in flowing air in a muffle furnace to drive the oxidation of $RuCl_3$ to RuO_2 [26]. After calcination, the catalyst was marked unwashed. Thus, the catalysts were referred to as Ru/TiO_2-M-uw where 'M' represents the nominal metal loading (wt%) of Ru and 'uw' identifies the sample as unwashed. For comparison, half of the obtained unwashed catalyst was exposed to an aqueous ammonia wash. During the washing step each sample was washed with 500 ml·g_{cat}^{-1} of 0.1 M NH_4OH over 5 min. Afterwards, the catalyst was rinsed with 500 ml of water and 0.200 g of $AgNO_3$ was added to the effluent to visually assess the presence of chlorine compounds. No cloudiness was observed after the washing treatment, indicating no additional chlorine removal occurred during the rinse. Catalysts were then dried at 110 °C and marked Ru/TiO_2-M-w ('w' indicates the washed catalyst). Complete experimental details are provided in Table S1.

2.3. Catalyst testing

A plug flow microreactor (Micromeritics, Effi) was used to evaluate catalyst activity. In a typical experiment, 0.100 g of catalyst and 0.500 g of SiO_2 were mixed and supported on an internal stainless-steel frit within a stainless-steel reactor tube (9 mm inner diameter). A K-type thermocouple, resting in the bed of catalyst, controlled the clamshell furnace temperature. Mass flow controllers delivered the reaction gases. An online Fourier transform infrared (FTIR) detector (California Analytical Instruments, 600 FTIR) continuously monitored effluent gas concentrations. Catalysts were reduced *in situ* by heating from 25 °C to 300 °C (ramp = 10 °C·min^{-1}, hold = 60 min) under 20 sccm H_2 and 180 sccm Ar. After cooling to 100 °C, the catalyst was bypassed and reactive gases began to flow to the online FTIR detector at 10 sccm CO_2, 50 sccm H_2, and 140 sccm Ar for 30 min to establish a stable feed composition. Once a stable signal was obtained (30 min), reactive gas was sent to the catalyst. The reactor was then heated in increments of 25 °C and held for 30 min at each temperature until 300 °C (ramp = 10 °C·min^{-1}) to obtain steady state CO_2 conversion. In all experiments, CH_4 was the only product observed with no CO detected, thus the selectivity for CH_4 was 100%. Carbon balances were between 99 % and 101 %. Fractional conversion of CO_2 was calculated from Eq. 2,

$$X = \frac{F_{CO_2,in} - F_{CO_2,out}}{F_{CO_2,in}} \tag{2}$$

where F_{CO_2} was the molar flowrate of CO_2 (mol CO_2·s^{-1}) obtained from the IR detector. Site-time yield (STY) to CH_4 (mol CH_4·(mol Ru·s)$^{-1}$) was calculated by Eq. 3,

$$STY_{CH_4} = \frac{F_{CO_2,in} \bullet X}{g_{cat} * \frac{M}{100} * \frac{1}{Ru_{AM}}} \tag{3}$$

where g_{cat} was the mass of catalyst (g), M was the nominal metal loading of Ru (wt%) and Ru_{AM} was the atomic mass of ruthenium (101.07 g·mol^{-1}).

2.4. Characterization methods and details

All characterization experiments were conducted on calcined materials, unless otherwise stated. Powder X-ray diffraction (PXRD) data were collected (Rigaku Corporation, Ultima IV) with Cu Kα source (40 kV, 44 mA). Diffraction patterns were collected in the 2θ range of 20–80° at a scan rate of 4°·min^{-1}.

X-ray photoelectron spectroscopy (XPS) data provided elemental ratios of Ti, Cl, and Ru (PHI, VersaProbe III model 5000). Samples were crushed into a fine powder and pressed onto conductive carbon tape. The tape was placed on a gold coated quartz slide for analysis. XPS data were obtained using Al Kα radiation. XPS spectra were calibrated with a Au standard material, which was cleaned *via* Ar-ion sputtering *in situ*.

The raw atomic ratios had an estimated ± 5% error due to surface inhomogeneities, surface roughness, and literature sensitivity values for peak integration.

Nitrogen physisorption (N_2-physisorption) isotherms were collected at − 196 °C (Quantachrome Instruments, Quadrasorb). Approximately 0.25 g of sample was weighed into clean/dry sample tubes. A filler rod was added to displace dead volume. Prior to analysis, samples were degassed under vacuum for 6 h at 200 °C. After degassing, samples were re-weighed to evaluate the removal of water and physisorbed species. The final dry mass was recorded and used to normalize the nitrogen physisorption quantities. Specific surface area (SSA) was determined using the Brunauer−Emmett−Teller (BET) method and was evaluated for consistency with the Rouquerol criteria (Table S2) [27]. Total pore volume was evaluated at a relative pressure of $P/P_0 = 0.98$ [28]. The surface area and pore volume measurements had an estimated error of ± 5 % due to small variations in sample mass.

Temperature programmed reduction (TPR) was evaluated using a temperature-controlled system (Altamira Instruments, Altamira-300) equipped with an online thermal conductivity detector (TCD). Prior to analysis, a clean/dry quartz U-tube was loaded with a plug of quartz wool. The plug was adjusted to the same height as the thermocouple (located on the outlet side of the tube). Samples were weighed (0.050–0.150 g) and loaded. An adjustable clamshell furnace was secured around the U-tube and the height was confirmed to be the same for all samples. All flowrates were 50 sccm and ramp rates were 10 °C·min^{-1}. Samples were heated to 300 °C in He (hold = 60 min) to remove adsorbed moisture and contaminants. The sample was then cooled to 30 °C in He. Once the temperature stabilized at 30 °C, flow of 4 % H_2/Ar was started. The sample was heated to 300 °C and reduction was measured by H_2 consumption on the TCD. Water, formed during the reduction, was removed from the stream using a dry ice trap. After reduction, the sample was held at 300 °C under Ar flow for 60 min to remove gas phase and surface bound hydrogen. The sample was then cooled to 50 °C in Ar prior to pulsed chemisorption of H_2 (pulses of 1 ml, 4 % H_2/Ar). Chemisorbed quantities of hydrogen (H_2-chemisorption) were calculated as the difference between the pulse area and breakthrough area (assigned as the point when the pulse area increased by less than 5 %). Chemisorption measurements had an estimated error of ± 5 % due to small variations in sample mass.

Selected samples were evaluated by diffuse reflectance Fourier transform infrared spectroscopy (DRIFTS). DRIFTS spectra were collected using an FTIR detector (Thermo-Nicolet, iS50) equipped with a heated sample cell (Harrick, Praying Mantis). A sample of dehydrated KBr in flowing N_2 at 25 °C was used as the background and subtracted from each spectrum. The spectra were acquired using 32 scans at a resolution of 4 cm^{-1}. During each experiment, the sample was pretreated with 2.5 % H_2/N_2 (200 sccm) while ramping at 10 °C·min^{-1} to 300 °C and holding for 60 min before cooling to 25 °C. Gas flows were then switched to 5 % H_2/N_2 (100 sccm) and 1 % CO_2/He (100 sccm), to obtain a 5:1 ratio of H_2:CO_2. Samples were then heated in 25 °C increments to 250 °C, ramping at 10 °C·min^{-1} between each setpoint and holding at each temperature for ~7 min to obtain the spectra.

Selected samples were imaged with transmission electron microscopy (TEM) and scanning TEM with energy dispersive X-ray spectroscopy (STEM-EDS). For particle size analysis, samples were reduced *ex situ* at 300 °C in 4 % H_2 for 60 min. Samples were then drop-cast onto carbon-coated copper grids (Ted Pella part no. 01824) or Lacey Carbon (Ted Pella part no. 01895-F) from an aqueous suspension. Imaging was performed (FEI Company, Tecnai G²-30) at 300 kV. Image analysis was conducted using the ImageJ software [29]. Ru particle size distributions were manually measured on ~100 particles.

A TGA (Setaram, SETSYS Evolution) provided the composition of the of $RuCl_3{\cdot}xH_2O$ precursor used in catalyst synthesis. Specifically, 0.050 g of $RuCl_3{\cdot}xH_2O$ was loaded and 50 sccm of N_2 flow was established. The sample was then heated to 950 °C at 10 °C·min^{-1}.

Scanning electron microscopy-energy dispersive X-ray spectroscopy (SEM-EDS) was performed (Evex, Mini-SEM) at an accelerating voltage of 20 kV to obtain the composition of the washed catalysts. The Ru Lα (2.60 keV) and Ti Kα (4.51 keV) emission lines were used to quantify the molar ratios of Ru and Ti. Due to the EDS overlap between Ru Lα and Cl Kα (2.62 keV), only the washed (Cl-removed) samples were analyzed to minimize the impact of convoluted Ru and Cl signals. EDS was conducted at several spots for each sample at a 50× magnification, which constituted an area of ~2 mm × 2 mm (~30 catalyst particles), giving an average molar Ru/Ti ratio.

2.5. Computational methods and details

All density functional theory (DFT) based simulations were performed using the Vienna *ab initio* Simulation Packages (VASP) code [30–33] and employed the RPBE functional [34]. Projector augmented wave potentials [35,36] were used for core-valence treatment with the plane-wave cutoff energy set to 400 eV. The Brillouin zone sampling was performed using a 4 × 4 × 1 Monkhorst-Pack [37] k-point grid. The Gaussian smearing scheme with a width of 0.1 eV was utilized for surfaces. Geometry optimizations were conducted with a self-consistent electronic convergence limit of 1 × 10^{-8} eV and an ionic convergence limit of 0.05 eV·Å^{-1} for unconstrained atoms. Periodic surface slabs of close-packed *hcp*-Ru (*0001*) and stepped *hcp*-Ru ($10\bar{1}0$) facets were constructed with a thickness of three layers and unit cell sizes of 3 × 3 (9 surface atoms) and 2 × 2 (4 surface atoms) to compute the Cl coverage dependence on the formation energies of CO_2. The bottom two layers of all surface slabs were held fixed at the optimized bulk lattice constant while the top layer was allowed to relax until convergence. Dipole corrections were applied in the surface-normal direction to all periodic surface slabs.

To investigate the effect of adsorbed chlorine contaminants on the stability of adsorbed CO_2, the formation energies of CO_2 was computed in the absence of adsorbed chlorine (0 monolayer (ML) Cl*) and at increasing Cl coverages of 1/9 ML and 1/4 ML on the Ru (*0001*) and 1/3 ML on the Ru ($10\bar{1}0$) surfaces. Calculations showed that Cl stably absorbed in the three-fold hollow site of Ru (*0001*) and ($10\bar{1}0$) surfaces. Stable configuration site sampling of CO_2 adsorption was evaluated on high symmetry Ru sites with adsorbed Cl present and absent on the Ru surfaces. The binding energy of CO_2 and H_2 on Ru were computed using elemental formation energies of C, H and O, where the C formation energy was referenced to $CH_{4(g)} - 2\,H_{2(g)}$, H was referenced to $1/2\,H_{2(g)}$, and O was referenced to $H_2O - 2\,H_{2(g)}$.

3. Results and discussion

Incipient wetness impregnation of $RuCl_3$ on TiO_2 was utilized to synthesize Ru/TiO_2 catalysts. The crystalline phase composition of the calcined low (Ru/TiO_2-1.0), medium (Ru/TiO_2-2.5), and high (Ru/TiO_2-5.0) loading Ru/TiO_2 catalysts, unwashed (uw) or washed (w) with aqueous ammonia, was assessed using PXRD. PXRD indicated the presence of the same crystalline phases for both the unwashed and washed materials after calcination (Fig. 1). For both the unwashed and washed samples, only reflections associated with the parent TiO_2 support were observed (10.8 % rutile, balance anatase). No additional reflections associated with crystalline RuO_2 species were observed, suggesting a high dispersion of Ru nanoparticles across all three metal loadings for both the unwashed and washed samples.

N_2-physisorption isotherms were collected to evaluate the catalyst surface area and pore volume (Fig. S2). All samples exhibited type II isotherms ascribed to the presence of a small quantity of micropores (low pressure knee) followed by monolayer and multilayer adsorption as the relative pressure approached $P/P_0 = 1$. Compared to the TiO_2 support, surface areas slightly decreased with the addition of Ru (Table 1) due to the increased sample density owed to increasing Ru content.

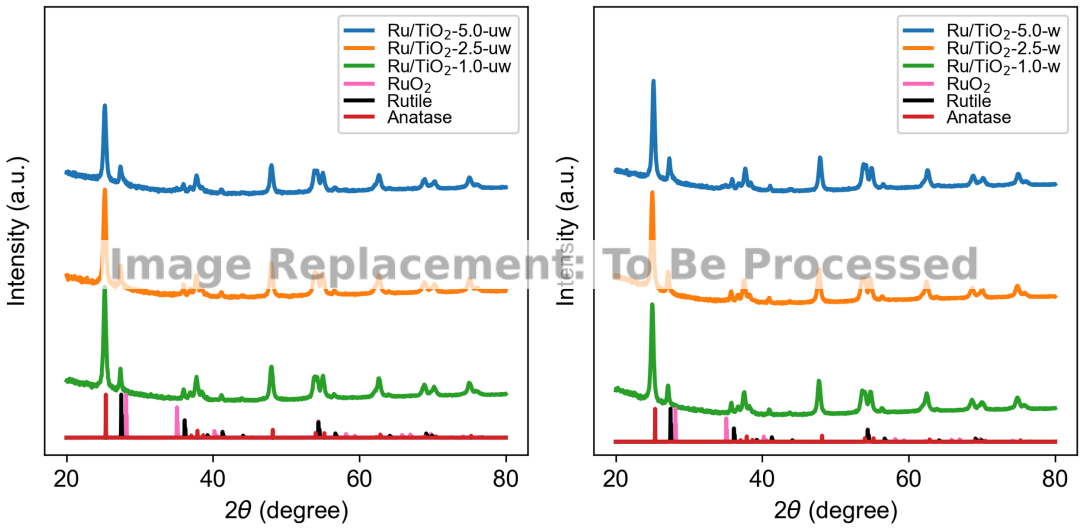

Fig. 1. Diffractograms of unwashed (left) and washed (right) Ru/TiO_2 catalysts after calcination. Calculated diffraction patterns for anatase, rutile, and RuO_2 phases are included for reference.

Table 1
Physicochemical properties of the unwashed and washed catalysts by XPS and N_2-physisorption.

	Ru/Ti ratio [(a)]		Cl/Ti ratio [(a)]		SSA($m^2 \cdot g_{cat}^{-1}$) [(b)]		V_{pore} ($cm^3 \cdot g_{cat}^{-1}$) [(c)]	
Catalyst	*uw*	*w*	*uw*	*w*	*uw*	*w*	*uw*	*w*
TiO_2	0.000	-	0.010	-	52	-	0.36	-
Ru/TiO_2-1.0	0.023	0.018	0.025	0.007	49	51	0.34	0.35
Ru/TiO_2-2.5	0.038	0.040	0.024	0.006	49	51	0.34	0.35
Ru/TiO_2-5.0	0.054	0.047	0.031	0.013	48	49	0.32	0.33
Ru/TiO_2-2.5-red	0.032	0.035	0.033	0.011	-	-	-	-

[(a)]High-resolution Cl 2p, Ru 3d, and Ti 2p XPS;
[(b)]Specific surface area calculated using the BET criteria;
[(c)]Total pore volume calculated a $P/P_0 = 0.98$. Dash (-) indicates that quantities were not measured.

Washed catalysts had slightly higher surface areas and pore volumes compared to unwashed catalysts but were within the experimental error of the measurement. Collectively, the results from PXRD and N_2-physisorption indicated that the unwashed and washed catalysts were crystallographically and structurally similar; the addition of increased ruthenium did not result in bulky crystallites or pore blockage.

Catalyst composition was estimated using SEM-EDS on the washed samples. The obtained Ru loading was close to the anticipated quantity (Fig. S3). The surface composition of Ru and Cl was evaluated by XPS. The bare TiO_2 had a small native quantity of Cl (Table 1) which was attributed to the TiO_2 chloride process [38]. For the Ru/TiO_2 catalysts the chlorine content, shown in the Cl 2p region, drastically decreased after washing (Fig. 2). The signal around 198.9 eV was assigned to chloride species, which is consistent with the presence of ruthenium chlorides [39]. For the Ru/TiO_2-1.0 and Ru/TiO_2-2.5 catalysts, complete removal of Cl was achieved by washing (comparing the Cl/Ti values in Table 1: $[Cl/Ti_{uw} - [Cl/Ti_w - Cl/Ti_{TiO_2,uw}]] \cdot [Cl/Ti_{uw}]^{-1} \cdot 100$ %). For the Ru/TiO_2-5.0 catalyst, *ca.* 90 % of Cl was removed. A reduced sample (Ru/TiO_2-2.5-(uw/w)-red, note: "red" is an abbreviation for "reduced") was also

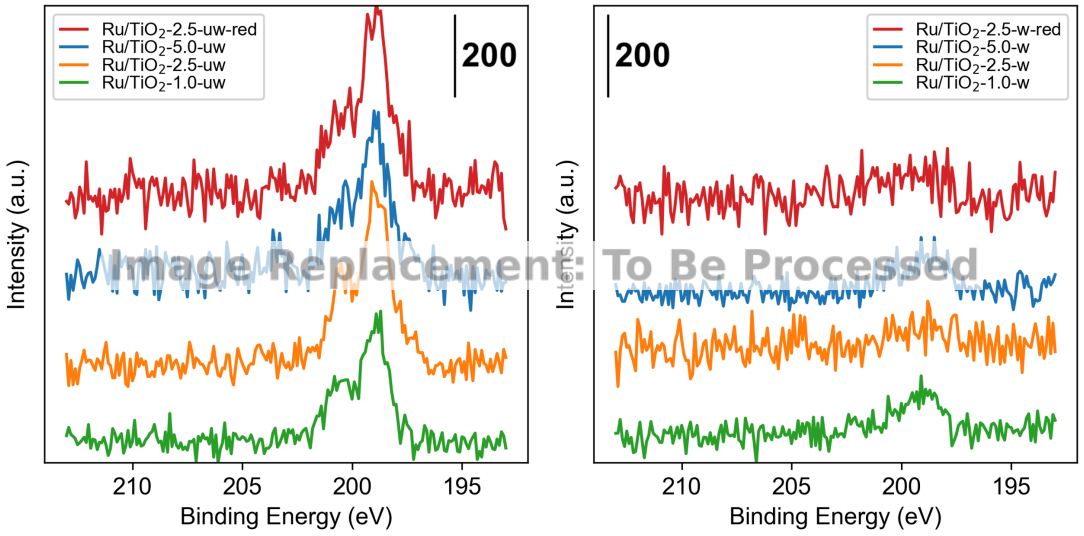

Fig. 2. XPS spectra of the Cl 2p region for unwashed (left), washed (right), and reduced Ru/TiO_2 catalysts. Note: "red" is an abbreviation for "reduced".

evaluated by XPS. After reducing at 300 °C in 4 % H_2 for 60 min, no significant change in the Cl signal intensity was observed when comparing (i) unreduced-unwashed to reduced-unwashed samples and (ii) unreduced-washed to reduced-washed samples. Thus, Cl removal was promoted by the aqueous ammonia wash and not, to an observable extent, by reduction at 300 °C. In the Ru 3d region (Fig. S4) increasing intensity of the Ru $3d_{5/2}$ peak near 280.9 eV and 280.7 eV for the respective unwashed and washed catalysts evidenced increasing surface concentration of Ru at higher loadings. Thus, a minimal loss of Ru was observed after washing the catalysts (Table 1). The 0.2 eV downshift in the Ru $3d_{5/2}$ peak after washing was consistent across all samples. The downward shift in binding energy after washing indicated that the Ru species were partially reduced, which could be related to the removal of Cl species (Binding energies for unsupported $RuCl_3$, RuO_3, RuO_2, Ru are 282.4, 282.38, 281.37, and 279.75 eV, respectively) [39]. In the Ti 2p region (Fig. S5) peaks blue-shifted (0.2 eV) for the washed catalysts. Similar Ru induced electronic modifications on TiO_2 have been attributed to higher electron charge density at Ti atoms and non-stoichiometric bonding of Ti to O with Ru substitution into the TiO_2 lattice [40]. After reduction at 300 °C, however, the peak location returned to 459.5 eV, indicating that the interaction induced by Ru addition and washing on TiO_2 was not retained after reduction.

TPR served as a measure of reducible Ru species and as an indication of the ease of overall H_2 activation (Fig. 3). Generally, the reduction features were attributed to H_2 consumption by RuO_2 or RuO_x located on either rutile or anatase TiO_2 [41]. Unwashed materials showed three reduction features centered around 115 °C (T_{low}), 155 °C (T_{med}), and 190 °C (T_{high}). After washing, T_{low} shifted *ca.* − 20 °C for all samples. T_{med} and T_{high} shifted to various degrees depending on the loading of the sample. Notably, T_{med} downshifted by *ca.* -25 °C for Ru/TiO_2-5.0-w. T_{high}, however, was consistently at *ca.* 190 °C. Wang and coworkers evaluated the reduction of Ru/TiO_2 on phase pure anatase and rutile TiO_2 supports. For anatase Ru/TiO_2, reduction features were observed at 128 and 150 °C and attributed to surface RuO_2 and interfacial RuO_x, respectively. On rutile Ru/TiO_2, reduction features were observed at 138 and 185 °C attributed to surface RuO_2 and interfacial RuO_x species, respectively [4]. In the current report, the TiO_2 support was a phase mixture of anatase and rutile (*see* Fig. 1). Thus, the T_{low} feature was tentatively assigned to surface RuO_2 species on either anatase or rutile TiO_2. The T_{med} and T_{high} features were assigned to interfacial RuO_x species on either anatase or rutile TiO_2.

The downshifting reduction temperatures for the majority of reducible Ru on washed catalysts indicated that the removal of chlorine enabled more facile H_2 activation. Similar behavior has been noted in the context of chlorine-contaminated cobalt catalysts [42]. The quantity of H_2 consumed by the unwashed (Ru/TiO_2-1.0-uw, Ru/TiO_2-2.5-uw, Ru/TiO_2-5.0-uw: 122, 277, 610 μmol·g^{-1}, respectively) and washed (Ru/TiO_2-1.0-w, Ru/TiO_2-2.5-w, Ru/TiO_2-5.0-w: 123, 268, 605 μmol·g^{-1}, respectively) materials during TPR were remarkably similar. This result provided confirmation that the total quantity of reducible Ru was not impacted by washing, however, the H_2 dissociation activity of the washed Ru sites was greatly improved.

The Ru/TiO_2 catalysts were tested for methanation at steady state conditions. Catalysts were first reduced *in situ* at 300 °C in flowing 10 % H_2. After cooling, a flow of 5:1 H_2:CO_2 in Ar provided a stoichiometric excess of H_2 for the methanation reaction. At this stoichiometric condition equilibrium CO_2 conversion can reach up to 100 % until roughly 300 °C; above 300 °C losses in CO_2 conversion and selectivity trade-offs to CO are probable (Fig. S6). The CO_2 conversion for the Ru/TiO_2 catalysts ranged from 0 % to 55 % across the studied temperature range. Therefore, no equilibrium conversion limitations were observed. Upon heating, reduction of carbon dioxide to methane was first observed at 200 °C for the Ru/TiO_2-1.0-uw catalyst (Fig. 4). The only observed products during the reaction were CH_4 and H_2O. Activity trends, by measure of STY (mol CH_4·(mol Ru·s)$^{-1}$), were Ru/TiO_2-1.0-uw > Ru/TiO_2-2.5-uw > Ru/TiO_2-5.0-uw. The same activity trend was observed for washed catalysts, where Ru/TiO_2-1.0-w was the most active and Ru/TiO_2-5.0-w was the least. The activity trends were attributed to the degree of ruthenium dispersion (Table 2), discussed in greater detail below. As the reaction temperature increased, methane STY continued to increase. The washed catalysts began converting CO_2 to CH_4 around 150 °C (~50 °C lower than the unwashed catalysts). The apparent activation energies for unwashed and washed catalysts were calculated from Arrhenius plots (Fig. 5). The average E_{app} for the unwashed and washed catalysts between 200 and 275 °C was 63.7 ± 1.5 and 54.7 ± 2.3 kJ·mol^{-1}, respectively. The obtained apparent activation energy values are close to those previously reported for Ru/TiO_2 catalysts [4,43]. Comparing the STY of unwashed and washed catalysts of equivalent metal loading, activity was most significantly improved at ~225 °C (Fig. S7). At 225 °C, the STY for Ru/TiO_2-1.0-w and Ru/TiO_2-2.5-w improved ~4.5 fold compared to the respective unwashed catalysts; the STY for the Ru/TiO_2-5.0-w improved ~3.5 fold compared to the Ru/TiO_2-5.0-uw catalyst. As the temperature increased past 225 °C,

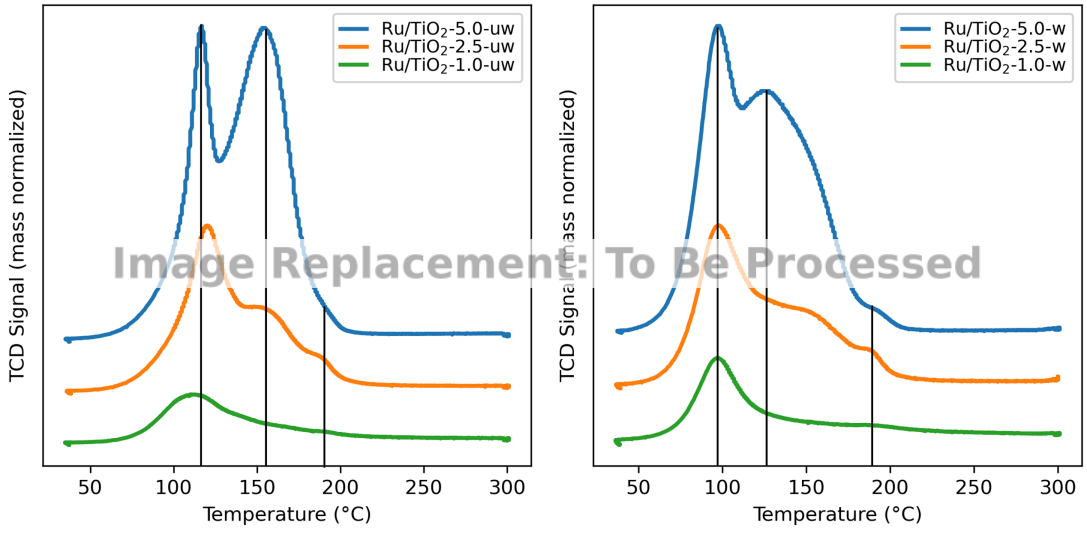

Fig. 3. Temperature programmed reduction of unwashed (left) and washed (right) Ru/TiO_2 catalysts. Vertical lines give reference to the temperature of the respective peak maximum.

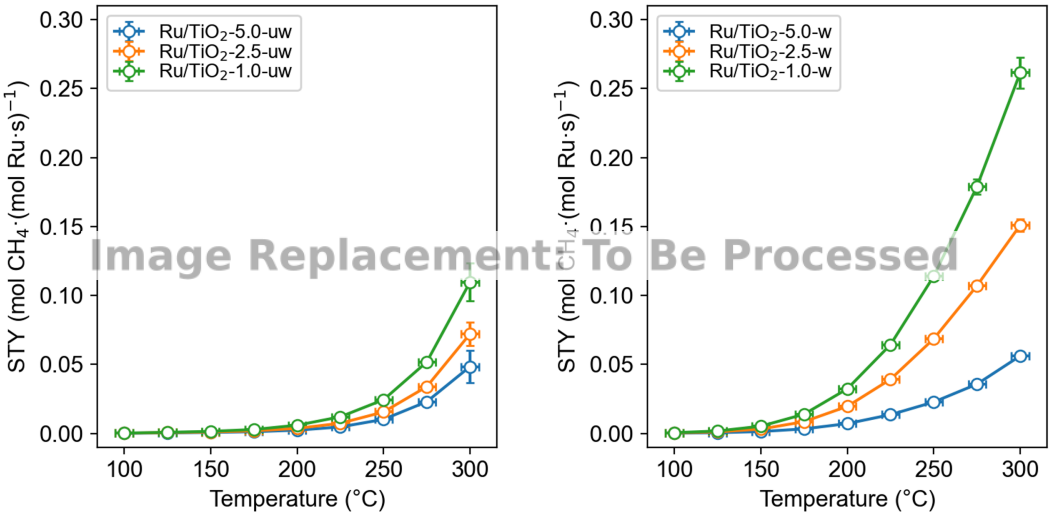

Fig. 4. Steady state CH_4 site-time yield for unwashed (left) and washed (right) Ru/TiO_2 catalysts at increasing reaction temperatures. Conditions: 0.100 g catalyst, 10 sccm CO_2, 50 sccm H_2, and 140 sccm Ar, 0.84 bar total pressure. Vertical error bars represent the range of STY over the 30 min hold at each temperature. Horizontal error bars represent temperature deviations during each 30 min hold.

Table 2
Pulsed hydrogen chemisorption results at 50 °C.

	H_2 uptake (μmol·g^{-1}) [a]		H/Ru ratio	
Catalyst	*uw*	*w*	*uw*	*w*
Ru/TiO_2-1.0	7.6	32.7	0.15	0.66
Ru/TiO_2-2.5	9.8	41.0	0.08	0.34
Ru/TiO_2-5.0	4.0	26.9	0.02	0.10

[a]Calculated from H_2-chemisorption.

relative activity improvements were less pronounced, which indicated that the poisoning effect of Cl may be overcome at higher temperatures. Although activity improvements were not as drastic at higher temperatures, the washed samples outperformed the unwashed samples up to the maximum evaluated temperature.

Overall, the removal of Cl was determined to be the main difference between the unwashed and washed catalysts. XPS indicated that the washing step was far more effective at removing chlorine species compared to reduction of the catalyst at 300 °C in flowing H_2. This result is well aligned with previous findings for Ru/Al_2O_3 catalysts (synthesized from $RuCl_3$) where an aqueous ammonia wash was more effective than thermal reduction up to 730 °C in flowing H_2 [44]. Thus, an aqueous ammonia wash presents a potential synthetic advantage compared to high temperature reduction as metal particle agglomeration [45] or strong metal-support interactions [46] are avoided. Furthermore, washing with aqueous ammonia is also reportedly more effective than washing with water [14]. Previous studies, however, do not provide a mechanism for chlorine removal from the catalyst surface during the aqueous ammonia wash. A possible mechanisms for the removal of Cl from various metal/metal oxide systems during the aqueous ammonia wash is proposed: Upon addition of the 0.1 M aqueous ammonia solution (pH ~ 11), the point of zero charge (PZC: the pH where the net charge of the particle surface is neutral) is surpassed (PZC for TiO_2 ~ 6, Al_2O_3 ~ 9, SiO_2 ~ 2) [47] and the catalyst surface becomes more negatively

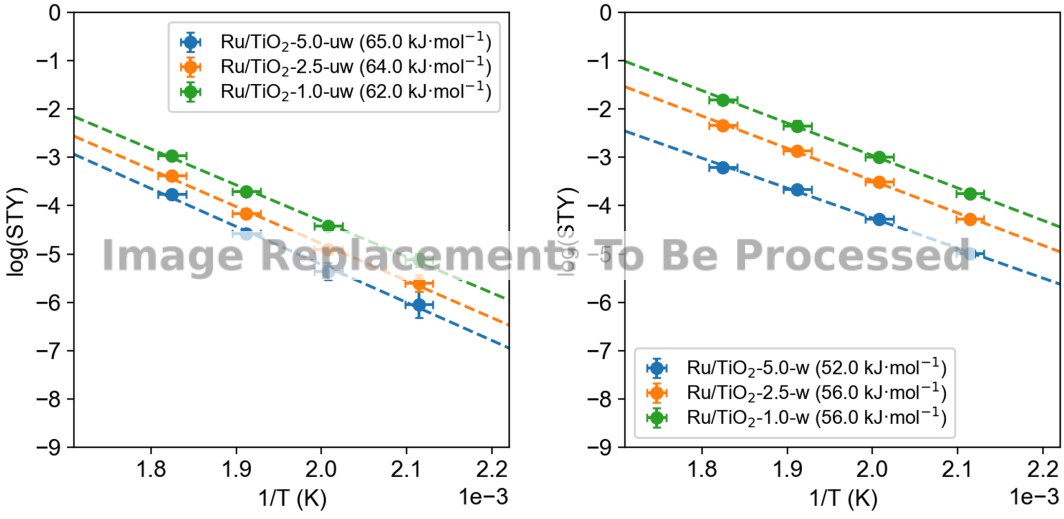

Fig. 5. Arrhenius plots from 200° to 275 °C for unwashed (left) and washed (right) Ru/TiO_2 catalysts. Vertical error bars represent propagated error from STY measurements. Horizontal error bars represent temperature deviation during each measurement. Linear fits (dashed lines) with $R^2 \geq 0.994$. Conditions: see Fig. 4.

charged as the metal/metal oxide surface is deprotonated [48,49]. Thus, negatively charged species (*e.g.*, chlorine) would be repelled and positively charged species (*e.g.*, RuO_x) [50] would be retained on the support.

To better understand the reason for the pronounced activity differences, further characterization was employed. The distribution of Ru nanoparticle sizes of the unwashed and washed Ru/TiO_2-1.0 catalysts were evaluated by TEM and found to be 1.1 ± 0.2 nm and 1.8 ± 1.4 nm, respectively (Fig. S8). The measured nanoparticle sizes were comparable to previously reported Ru particles on mixed phase TiO_2 [51,52].

H_2-chemisorption provided an estimation of the Ru exposure of the unwashed and washed Ru/TiO_2 catalysts. Note that characterization of ruthenium active sites on titania has proven challenging by CO-chemisorption [53] (due to particle size dependent CO:Ru ratios) and by H_2-chemisorption [54] (owed to the possibility of strong metal-support interactions between Ru and TiO_2). Of the two methods, H_2-chemisorption is generally preferred [54,55]. Additionally, the presence of electronegative Cl modifies the H_2 dissociation properties of the supported Ru catalysts. Several previous studies report that the presence of Cl adatoms on high coordination sites or at increasing coverage on the Ru surface can promote a site-blocking or electronic modulation of the Ru atoms decreasing the overall adsorption strength of hydrogen during dissociative chemisorption [13,55–57]. Thus, H_2-chemisorption convolves the dispersion of Ru and the amount of residual Cl at Ru sites. Therefore, the H_2-chemisorption results were treated as qualitative and were not used to evaluate the dispersion (or turnover frequency) of Ru. Generally, it was clear that washed catalysts had significantly higher hydrogen uptake as compared to the unwashed catalysts (Table 2). The increase in H/Ru ratio was approximately 4-fold for all washed catalysts, which roughly correlates with the observed activity improvements during methanation. Furthermore, H/Ru increased at lower metal loadings, owed to increased metal surface area. The lower H_2 adsorption on Cl-contaminated Ru/TiO_2 catalysts correlated well with previous findings.

To further probe CO_2 activation under reaction conditions, DRIFTS experiments were conducted on the unwashed and washed catalysts during *in situ* CO_2 methanation at 200 °C (Fig. 6). The washed catalysts (Ru/TiO_2-1.0-w and Ru/TiO_2-5.0-w) exhibited significantly more pronounced signals in the CO stretching region (1800–2200 cm^{-1}) than the unwashed catalysts (Ru/TiO_2-1.0-uw and Ru/TiO_2-5.0-uw). Additionally, the enhancement of the CO stretching region was much more obvious on the Ru/TiO_2-1.0-w catalysts. The vibration centered around 2000 cm^{-1} was assigned to linear CO bound to Ru. The small peak around 2075 cm^{-1} may be associated with either CO bound to positively charged, oxidized Ru sites [51], or geminal $Ru(CO)_2$ dicarbonyl species [4]. Many studies have hypothesized that CO is a key intermediate in the CO_2 methanation process [22,51]. Thus, enhanced CO formation over washed catalysts corroborates the steady state methanation experiments, where the washed catalysts demonstrated greater activity

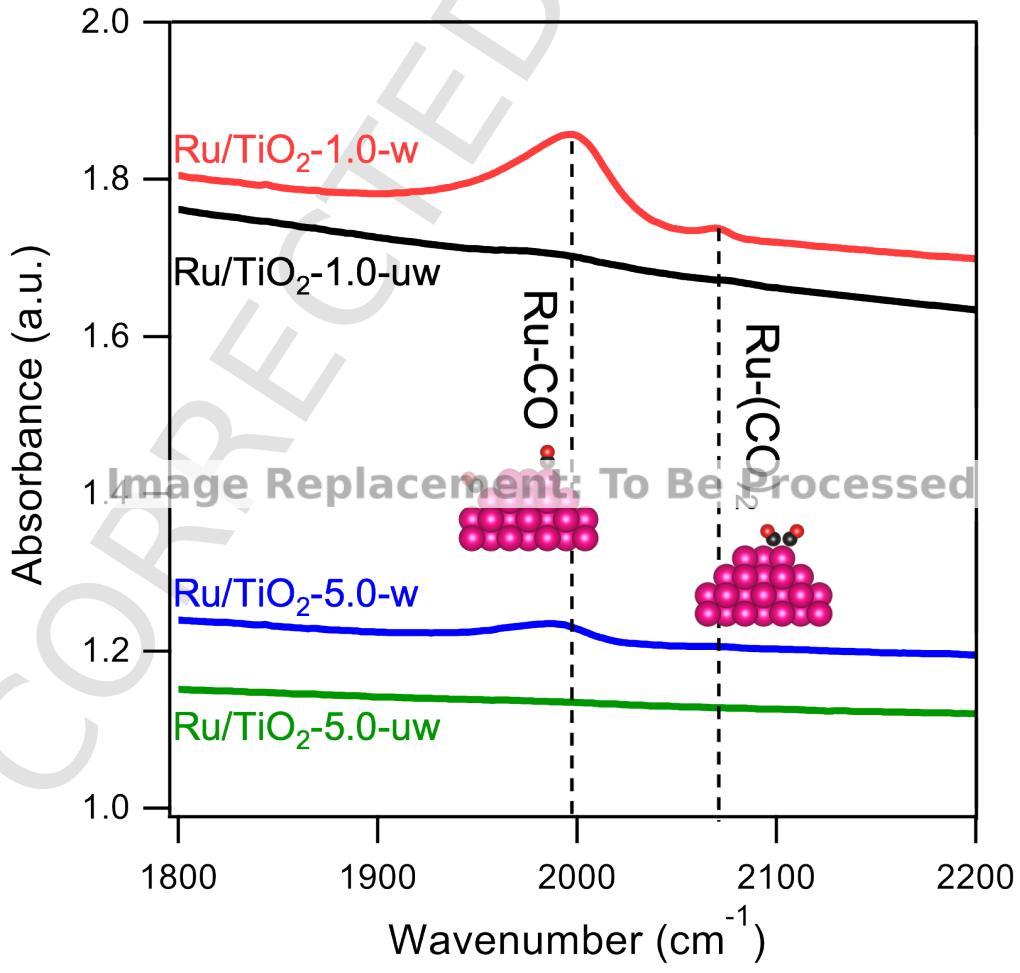

Fig. 6. DRIFTS spectra of Ru/TiO_2-1.0 and Ru/TiO_2-5.0 during *in situ* methanation. Conditions: 100 sccm 5 % H_2/N_2 and 100 sccm 1 % CO_2/He at 200 °C. Atom color representations: Ru (magenta), C (black), and O (red).

than the unwashed catalysts, and the extent of this improvement was more pronounced for Ru/TiO_2-1.0-w compared to Ru/TiO_2-5.0-w. Temperature dependent DRIFTS spectra were collected for each sample (Fig. S9). The onset of CO formation was room temperature for the Ru/TiO_2-1.0-w catalyst and ~75 °C for Ru/TiO_2-1.0-uw which roughly coincides with the shift in light-off temperature observed during the steady state methanation tests.

DFT calculations were conducted to evaluate CO_2 adsorption on Ru surfaces at 0, 1/9 and 1/4 ML of adsorbed Cl on close-packed *hcp*-Ru (*0001*) and at 0 ML and 1/3 ML on the flat hollow site in close-packed Ru ($10\bar{1}0$) surfaces to evaluate the qualitative effect of Cl contamination. The calculations indicated that CO_2 preferentially adsorbed at Ru bridge sites when no (0 ML) or low (1/9 ML) Cl coverage was present on the surface (Fig. 7). At higher Cl coverages (1/4 ML), however, the calculations showed that CO_2 was destabilized by 130 kJ·mol^{-1} indicating that higher concentrations of Cl contaminants contribute to weakening and inhibition of CO_2 binding on Ru surfaces. Moreover, CO_2 was found to adsorb even stronger at the step site on Ru ($10\bar{1}0$) than the flat hollow site in close-packed Ru (*0001*) ($\Delta G_{CO2^* \mid step} = -66$ kJ·mol^{-1} *versus* $\Delta G_{CO2^* \mid flat} = 34$ kJ·mol^{-1}, where negative ΔG denote stronger adsorption). In the presence of adsorbed Cl (1/3 ML) on stepped Ru, the binding energy of CO_2 was destabilized by 89 kJ·mol^{-1} compared to no Cl (0 ML) on Ru ($10\bar{1}0$) indicating that Cl could capably weaken even preferentially strong binding edge sites for CO_2. The calculations further showed that Cl energetically had the same edge adsorption site preference (step-bridge site of Ru ($10\bar{1}0$)) as CO_2. Based on these qualitative trends, it is postulated that Cl at higher contaminant concentrations likely competes for edge and other defect or under-coordinated sites on the Ru and blocks access for CO_2 adsorption. These computational results corroborate the findings from DRIFTS, which indicate that Cl blocks active sites that are essential for CO_2 adsorption and the methanation reaction.

4. Conclusions

An aqueous ammonia wash removed significant Cl quantities from Ru/TiO_2 catalysts (XPS). Unwashed catalysts were morphologically similar to washed catalysts (XRD, N_2-physisorption, TEM). The removal of Cl resulted in ~4.5x methanation activity boost for catalysts with small Ru nanoparticles at 225 °C. The observed improvement in activity was attributed to lower temperature activation of H_2 (TPR, H_2-chemisorption, DFT) and increased activation of CO_2 (DRIFTS). Chlorine and CO_2 preferentially occupy step sites on Ru nanoparticles (DFT), thus Cl removal increased CO_2 adsorption. Essentially, Cl blocks the active sites on Ru that are directly involved in the process of CO_2 hydrogenation. Removal of Cl contamination drastically improved the overall activity of the Ru/TiO_2 catalyst at low temperature. This study provides guidance for future catalyst syntheses and probes important contaminant-catalyst properties in the context of carbon dioxide utilization.

CRediT authorship contribution statement

James M. Crawford : Conceptualization, Investigation, Visualization, Supervision, Writing - original draft. **Brittney Petel :** Formal analysis, Methodology, Writing - review & editing. **Mathew J. Rasmussen :** Formal analysis, Methodology, Writing - review & editing. **Thomas Ludwig :** Formal analysis, Methodology, Writing - review & editing. **Elisa M. Miller :** Formal analysis, Methodology, Writing - review & editing. **Sneha A. Akhade :** Software, Writing - review & editing. **Simon H. Pang :** Funding acquisition, Supervision, Writing - review & editing. **Matthew Yung :** Funding acquisition, Supervision, Writing - original draft.

Declaration of Competing Interest

The authors declare that they have no known competing financial interests or personal relationships that could have appeared to influence the work reported in this paper.

Data Availability

Data will be made available on request.

Acknowledgments

The authors would like to acknowledge the financial support from the U.S. Department of Energy (DOE) Office of Fossil Energy and Carbon Management under grant FWP-FEW0277. This work was authored in part by the National Renewable Energy Laboratory, managed and operated by Alliance for Sustainable Energy, LLC, for the U.S. DOE under

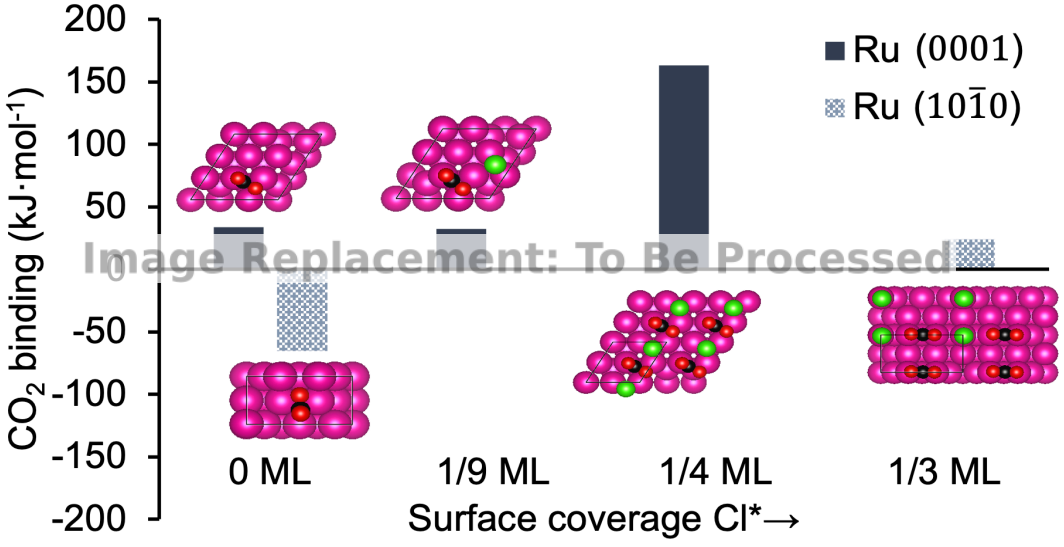

Fig. 7. Computed binding energies of CO_2 as a function of coverage of Cl adsorbed on close-packed Ru (*0001*) and stepped Ru ($10\bar{1}0$) surfaces. Positive energies denote weaker binding. Atom color representations: Ru (magenta), C (black), O (red) and Cl (green).

contract no. DE-AC36–08GO28308. Work at Lawrence Livermore National Laboratory was done under the auspices of the U.S. DOE under contract no. DE-AC52–07NA27344.

Appendix A. Supporting information

Supplementary data associated with this article can be found in the online version at doi:10.1016/j.apcata.2023.119292.

References

[1] C. Vogt, M. Monai, G.J. Kramer, B.M. Weckhuysen, The renaissance of the sabatier reaction and its applications on earth and in space, Nat. Catal. 2 (3) (2019) 188–197, https://doi.org/10.1038/s41929-019-0244-4.

[2] J. Ashok, S. Pati, P. Hongmanorom, Z. Tianxi, C. Junmei, S. Kawi, A review of recent catalyst advances in CO_2 methanation processes, Catal. Today 356 (2020) 471–489, https://doi.org/10.1016/j.cattod.2020.07.023.

[3] K.R. Thampi, J. Kiwi, M. Grätzel, Methanation and photo-methanation of carbon dioxide at room temperature and atmospheric pressure, Nature 327 (6122) (1987) 506–508, https://doi.org/10.1038/327506a0.

[4] J. Zhou, Z. Gao, G. Xiang, T. Zhai, Z. Liu, W. Zhao, X. Liang, L. Wang, Interfacial compatibility critically controls Ru/TiO_2 metal-support interaction modes in CO_2 hydrogenation, Nat. Commun. 13 (1) (2022) 327, https://doi.org/10.1038/s41467-021-27910-4.

[5] A. Kim, C. Sanchez, G. Patriarche, O. Ersen, S. Moldovan, A. Wisnet, C. Sassoye, P. Debecker, Selective CO_2 methanation on Ru/TiO_2 catalysts: unravelling the decisive role of the TiO_2 support crystal structure, Catal. Sci. Technol. 6 (22) (2016) 8117–8128, https://doi.org/10.1039/C6CY01677D.

[6] Y. Yan, Q. Wang, C. Jiang, Y. Yao, D. Lu, J. Zheng, Y. Dai, H. Wang, Y. Yang, Ru/Al_2O_3 catalyzed CO_2 hydrogenation: oxygen-exchange on metal-support interfaces, J. Catal. 367 (2018) 194–205, https://doi.org/10.1016/j.jcat.2018.08.026.

[7] Y. Zhang, W. Yan, H. Qi, X. Su, Y. Su, X. Liu, L. Li, X. Yang, Y. Huang, T. Zhang, Strong metal–support interaction of Ru on TiO_2 derived from the Co-reduction mechanism of Ru$Ti_{1-x}O_2$ interphase, ACS Catal. 12 (3) (2022) 1697–1705, https://doi.org/10.1021/acscatal.1c04785.

[8] S. Chai, Y. Men, J. Wang, S. Liu, Q. Song, W. An, G. Kolb, Boosting CO_2 methanation activity on Ru/TiO_2 catalysts by exposing (001) facets of anatase TiO_2, J. CO2 Util. 33 (2019) 242–252, https://doi.org/10.1016/j.jcou.2019.05.031.

[9] C. Zhou, A.S. Asundi, E.D. Goodman, J. Hong, B. Werghi, A.S. Hoffman, S.S. Nathan, S.F. Bent, S.R. Bare, M. Cargnello, Steering CO_2 hydrogenation toward C–C coupling to hydrocarbons using porous organic polymer/metal interfaces, Proc. Natl. Acad. Sci. USA 119 (7) (2022) e2114768119, https://doi.org/10.1073/pnas.2114768119.

[10] J. Zhang, S. Deo, M.J. Janik, J.W. Medlin, Control of molecular bonding strength on metal catalysts with organic monolayers for CO_2 reduction, J. Am. Chem. Soc. 142 (11) (2020) 5184–5193, https://doi.org/10.1021/jacs.9b12980.

[11] G.K. Schweitzer, L.L. Pesterfield, The Ti group and the 5B, 6B, 7B and 8B heavy elements, in: G.K. Schweitzer, L.L. Pesterfield (Eds.), The Aqueous Chemistry of the Elements, Oxford University Press, 2010, pp. 315–316, https://doi.org/10.1093/oso/9780195393354.003.0015.

[12] Y. Manaka, Y. Nagata, K. Kobayashi, D. Kobayashi, T. Nanba, The effect of a ruthenium precursor on the low-temperature ammonia synthesis activity over Ru/CeO_2, Dalton Trans. 49 (47) (2020) 17143–17146, https://doi.org/10.1039/D0DT01974G.

[13] B. Lin, R. Wang, J. Lin, J. Ni, K. Wei, Effect of chlorine on the chemisorptive properties and ammonia synthesis activity of alumina-supported Ru catalysts, Catal. Lett. 141 (10) (2011) 1557, https://doi.org/10.1007/s10562-011-0658-3.

[14] T. Nakamura, M. Ohshima, H. Kurokawa, H. Miura, Effects of removing residual chlorine on the hydrogenation of aromatic hydrocarbons over supported Ru catalysts, Chem. Lett. 39 (1) (2010) 62–63, https://doi.org/10.1246/cl.2010.62.

[15] G. Blondeel, A. Harriman, G. Porter, D. Urwin, J. Kiwi, Design, preparation and characterization of ruthenium dioxide/titanium dioxide catalytic surfaces active in photooxidation of water, J. Phys. Chem. 87 (14) (1983) 2629–2636, https://doi.org/10.1021/j100237a031.

[16] A.M. Abdel-Mageed, D. Widmann, S.E. Olesen, I. Chorkendorff, J. Biskupek, R.J. Behm, Selective CO methanation on Ru/TiO_2 catalysts: role and influence of metal–support interactions, ACS Catal. 5 (11) (2015) 6753–6763, https://doi.org/10.1021/acscatal.5b01520.

[17] S. Chen, A.M. Abdel-Mageed, D. Li, J. Bansmann, S. Cisneros, J. Biskupek, W. Huang, R.J. Behm, Morphology-engineered highly active and stable Ru/TiO_2 catalysts for selective CO methanation, Angew. Chem. Int. Ed. 58 (31) (2019) 10732–10736, https://doi.org/10.1002/anie.201903882.

[18] A.M. Abdel-Mageed, K. Wiese, M. Parlinska-Wojtan, J. Rabeah, A. Brückner, R.J. Behm, Encapsulation of Ru nanoparticles: modifying the reactivity toward CO and CO_2 methanation on highly active Ru/TiO_2 catalysts, Appl. Catal. B Environ. 270 (2020) 118846, https://doi.org/10.1016/j.apcatb.2020.118846.

[19] Z. Zhao, Q. Jiang, Q. Wang, M. Wang, J. Zuo, H. Chen, Q. Kuang, Z. Xie, Effect of rutile content on the catalytic performance of Ru/TiO_2 catalyst for low-temperature CO_2 methanation, ACS Sustain. Chem. Eng. 9 (42) (2021) 14288–14296, https://doi.org/10.1021/acssuschemeng.1c05565.

[20] P. Dongapure, S. Bagchi, S. Mayadevi, R.N. Devi, Variations in activity of Ru/TiO_2 and Ru/Al_2O_3 catalysts for CO_2 hydrogenation: an investigation by in-situ infrared spectroscopy studies, Mol. Catal. 482 (2020) 110700, https://doi.org/10.1016/j.mcat.2019.110700.

[21] U. Caudillo-Flores, G. Agostini, C. Marini, A. Kubacka, M. Fernández-García, Hydrogen thermo-photo production using Ru/TiO_2: heat and light synergistic effects, Appl. Catal. B Environ. 256 (2019) 117790, https://doi.org/10.1016/j.apcatb.2019.117790.

[22] J. Xu, X. Su, H. Duan, B. Hou, Q. Lin, X. Liu, X. Pan, G. Pei, H. Geng, Y. Huang, T. Zhang, Influence of pretreatment temperature on catalytic performance of rutile TiO_2-supported ruthenium catalyst in CO_2 methanation, J. Catal. 333 (2016) 227–237, https://doi.org/10.1016/j.jcat.2015.10.025.

[23] P. Panagiotopoulou, D.I. Kondarides, X.E. Verykios, Mechanistic aspects of the selective methanation of CO over Ru/TiO_2 catalyst, Catal. Today 181 (1) (2012) 138–147, https://doi.org/10.1016/j.cattod.2011.05.030.

[24] P. Panagiotopoulou, D.I. Kondarides, X.E. Verykios, Mechanistic study of the selective methanation of CO over Ru/TiO_2 catalyst: identification of active surface species and reaction pathways, J. Phys. Chem. C 115 (4) (2011) 1220–1230, https://doi.org/10.1021/jp106538z.

[25] W.K. Jóźwiak, T.P. Maniecki, Influence of atmosphere kind on temperature programmed decomposition of noble metal chlorides, Thermochim. Acta 435 (2) (2005) 151–161, https://doi.org/10.1016/j.tca.2005.05.006.

[26] A.E. Newkirk, D.W. McKee, Thermal decomposition of rhodium, iridium, and ruthenium chlorides, J. Catal. 11 (4) (1968) 370–377, https://doi.org/10.1016/0021-9517(68)90061-4.

[27] J. Rouquerol, P. Llewellyn, F. Rouquerol, Is the bet equation applicable to microporous adsorbents? in: P.L. Llewellyn, F. Rodriquez-Reinoso, J. Rouqerol, N. Seaton (Eds.), Studies in Surface Science and Catalysis. Characterization of Porous Solids VII, Vol. 160, Elsevier, 2007, pp. 49–56, https://doi.org/10.1016/S0167-2991(07)80008-5.

[28] E.P. Barrett, L.G. Joyner, Determination of nitrogen adsorption-desorption isotherms, Anal. Chem. 23 (5) (1951) 791–792, https://doi.org/10.1021/ac60053a032.

[29] C.A. Schneider, W.S. Rasband, K.W. Eliceiri, NIH image to imageJ: 25 years of image analysis, Nat. Methods 9 (7) (2012) 671–675, https://doi.org/10.1038/nmeth.2089.

[30] G. Kresse, J. Furthmüller, Efficiency of ab-initio total energy calculations for metals and semiconductors using a plane-wave basis set, Comput. Mater. Sci. 6 (1) (1996) 15–50, https://doi.org/10.1016/0927-0256(96)00008-0.

[31] G. Kresse, J. Furthmüller, Efficient iterative schemes for Ab initio total-energy calculations using a plane-wave basis set, Phys. Rev. B 54 (16) (1996) 11169–11186, https://doi.org/10.1103/PhysRevB.54.11169.

[32] G. Kresse, J. Hafner, Ab initio molecular-dynamics simulation of the liquid-metal--amorphous-semiconductor transition in germanium, Phys. Rev. B 49 (20) (1994) 14251–14269, https://doi.org/10.1103/PhysRevB.49.14251.

[33] G. Kresse, J. Hafner, Ab initio molecular dynamics for liquid metals, Phys. Rev. B 47 (1) (1993) 558–561, https://doi.org/10.1103/PhysRevB.47.558.

[34] B. Hammer, L.B. Hansen, J.K. Nørskov, Improved adsorption energetics within density-functional theory using revised Perdew-Burke-Ernzerhof functionals, Phys. Rev. B 59 (11) (1999) 7413–7421, https://doi.org/10.1103/PhysRevB.59.7413.

[35] G. Kresse, D. Joubert, From ultrasoft pseudopotentials to the projector augmented-wave method, Phys. Rev. B 59 (3) (1999) 1758–1775, https://doi.org/10.1103/PhysRevB.59.1758.

[36] P.E. Blöchl, Projector augmented-wave method, Phys. Rev. B 50 (24) (1994) 17953–17979, https://doi.org/10.1103/PhysRevB.50.17953.

[37] J.D. Pack, H.J. Monkhorst, Special points for brillouin-zone integrations" – a reply, Phys. Rev. B 16 (4) (1977) 1748–1749, https://doi.org/10.1103/PhysRevB.16.1748.

[38] Gonzalez, R.A.; Musick, C.D.; Tilton, J.N. Process for Controlling Agglomeration in the Manufacture of TiO2. US5508015A, April 16, 1996. https://patents.google.com/patent/US5508015A/en (accessed 2022–09-13).

[39] D.J. Morgan, Resolving ruthenium: XPS studies of common ruthenium materials, Surf. Interface Anal. 47 (11) (2015) 1072–1079, https://doi.org/10.1002/sia.5852.

[40] T.-D. Nguyen-Phan, S. Luo, D. Vovchok, J. Llorca, S. Sallis, S. Kattel, W. Xu, L.F.J. Piper, D.E. Polyansky, S.D. Senanayake, D.J. Stacchiola, J.A. Rodriguez, Three-dimensional ruthenium-doped TiO_2 sea urchins for enhanced visible-light-responsive H_2 production, Phys. Chem. Chem. Phys. 18 (23) (2016) 15972–15979, https://doi.org/10.1039/C6CP00472E.

[41] C. Hernandez-Mejia, E.S. Gnanakumar, A. Olivos-Suarez, J. Gascon, H.F. Greer, W. Zhou, G. Rothenberg, N.R. Shiju, Ru/TiO_2-catalysed hydrogenation of xylose: the role of the crystal structure of the support, Catal. Sci. Technol. 6 (2) (2016) 577–582, https://doi.org/10.1039/C5CY01005E.

[42] M. Li, F. Bi, Y. Xu, P. Hao, K. Xiang, Y. Zhang, S. Chen, J. Guo, X. Guo, W. Ding, Effect of residual chlorine on the catalytic performance of Co3O4 for CO oxidation, ACS Catal. 9 (12) (2019) 11676–11684, https://doi.org/10.1021/acscatal.9b03797.

[43] M.S. Duyar, A. Ramachandran, C. Wang, R.J. Farrauto, Kinetics of CO_2 methanation over Ru/γ-Al_2O_3 and implications for renewable energy storage applications, J. CO2 Util. 12 (2015) 27–33, https://doi.org/10.1016/j.jcou.2015.10.003.

[44] T. Narita, H. Miura, M. Ohira, H. Hondou, K. Sugiyama, T. Matsuda, R.D. Gonzalez, The effect of reduction temperature on the chemisorptive properties of Ru/Al_2O_3: effect of chlorine, Appl. Catal. 32 (1987) 185–190, https://doi.org/10.1016/S0166-9834(00)80624-7.

[45] B. Lin, K. Wei, J. Lin, J. Ni, Effect of treatment conditions on ruthenium particle size and ammonia synthesis activity of ruthenium catalyst, Catal. Commun. 39

(2013) 14–19, https://doi.org/10.1016/j.catcom.2013.05.003.
[46] T. Komaya, A.T. Bell, Z. Wengsieh, R. Gronsky, F. Engelke, T.S. King, M. Pruski, The influence of metal-support interactions on the accurate determination of Ru dispersion for Ru/TiO_2, J. Catal. 149 (1) (1994) 142–148, https://doi.org/10.1006/jcat.1994.1279.
[47] Jolivet, J.-P.; Henry, M.; Livage, J. Metal Oxide Chemistry and Synthesis: From Solution to Solid State; Wiley-Blackwell.
[48] K. Suttiponparnit, J. Jiang, M. Sahu, S. Suvachittanont, T. Charinpanitkul, P. Biswas, Role of surface area, primary particle size, and crystal phase on titanium dioxide nanoparticle dispersion properties, Nanoscale Res. Lett. 6 (1) (2010) 27, https://doi.org/10.1007/s11671-010-9772-1.
[49] L. Jiao, J.R. Regalbuto, The synthesis of highly dispersed noble and base metals on silica via strong electrostatic adsorption: I. amorphous silica, J. Catal. 260 (2) (2008) 329–341, https://doi.org/10.1016/j.jcat.2008.09.022.
[50] J. Yang, J.Y. Lee, T.C. Deivaraj, H.-P. Too, Preparation and characterization of positively charged ruthenium nanoparticles, J. Colloid Interface Sci. 271 (2) (2004) 308–312, https://doi.org/10.1016/j.jcis.2003.10.041.
[51] M.R. Prairie, A. Renken, J.G. Highfield, K. Ravindranathan Thampi, M. Grätzel, A fourier transform infrared spectroscopic study of CO_2 methanation on supported ruthenium, J. Catal. 129 (1) (1991) 130–144, https://doi.org/10.1016/0021-9517(91)90017-X.
[52] P. Ruterana, P.-A. Buffat, K.R. Thampi, M. Graetzel, Selective dispersion of the $Ru\text{-}RuO_x/TiO_2$ catalyst for methanation of CO_2 at room temperature and atmospheric pressure, MRS Online Proc. Libr 139 (1) (1988) 327–332, https://doi.org/10.1557/PROC-139-327.
[53] C.-H. Yang, J.G. Goodwin, Particle size dependence for CO chemisorption on supported Ru catalysts, React. Kinet. Catal. Lett. 20 (1) (1982) 13–18, https://doi.org/10.1007/BF02063576.
[54] Y.W. Chen, H.T. Wang, J.G. Goodwin, Effect of preparation methods on the catalytic properties of zeolite-supported ruthenium in the Fischer-Tropsch synthesis, J. Catal. 83 (2) (1983) 415–427, https://doi.org/10.1016/0021-9517(83)90066-0.
[55] K. Lu, B.J. Tatarchuk, Activated chemisorption of hydrogen on supported ruthenium: II. Effects of crystallite size and adsorbed chlorine on accurate surface area measurements, J. Catal. 106 (1) (1987) 176–187, https://doi.org/10.1016/0021-9517(87)90222-3.
[56] K. Lu, B.J. Tatarchuk, Activated chemisorption of hydrogen on supported ruthenium: I. Influence of adsorbed chlorine on accurate surface area measurements, J. Catal. 106 (1) (1987) 166–175, https://doi.org/10.1016/0021-9517(87)90221-1.
[57] X. Wu, B.C. Gerstein, T.S. King, The effect of chlorine on hydrogen chemisorption by silica-supported Ru catalysts: a proton NMR study, J. Catal. 135 (1) (1992) 68–80, https://doi.org/10.1016/0021-9517(92)90269-N.